CRYSTAL GROWTH & DESIGN

pubs.acs.org/crystal

Article

Mn(III) Chain Coordination Polymers Assembled by Salicylidene-2-ethanolamine Schiff Base Ligands: Synthesis, Crystal Structures, and HFEPR Study

Oleh Stetsiuk, Nataliya Plyuta, Narcis Avarvari, Evgeny Goreshnik, Vladimir Kokozay, Svitlana Petrusenko,* and Andrew Ozarowski*

Cite This: *Cryst. Growth Des.* 2020, 20, 1491−1502

Read Online

ACCESS | Metrics & More | Article Recommendations | Supporting Information

ABSTRACT: A family of eight polymeric manganese(III) complexes with the general formula $Mn(HL^{1,2})_2X$ (H_2L^1 = 2[(2-hydroxyethyl)iminomethyl]-phenol, H_2L^2 = 2[(2-hydroxyethyl)iminomethyl]-6-methoxy-phenol), while X = Cl (**1**, **5**), Br (**2**, **6**), I (**3**, **7**), NCS (**4**, **8**) for H_2L^1 and H_2L^2, respectively were obtained using "the direct synthesis" approach, i.e., the oxidative dissolution of the manganese powder in the presence of a Schiff base (SB), an ammonium salt, and oxygen in the air. Single crystal X-ray diffraction studies for the new complexes **2**, **3**, **4**, and **8** were compared with the previously reported crystallographic data for **1** and **7**, showing that all complexes possess a one-dimensional polymeric structure. The main structural units in **1**−**7** are cationic chains $[Mn(HL^{1,2})_2]_n^{n+}$ and anions X^- linked together via electrostatic interactions and hydrogen bonds, while the complex **8** consists of polymeric chains of neutral $[Mn(HL^2)_2(NCS)]_n$ units. The SB ligands are mono-deprotonated as HL^-, and coordinated by the metal atoms in a tridentate chelate-bridging fashion generating chains with Mn centers connected by double or single {−N−C−C−O−} bridges for **1**−**7** and **8**, respectively. In **8**, bridging and pure chelate modes of HL^{2-} occur. The intrachain $Mn^{III}\cdots Mn^{III}$ distances vary from 5.700(2) Å for **1** to 6.6950(4) Å for **8**. A high-field electron paramagnetic resonance study reveals narrow ranges of the zero-field splitting parameters of the spin Hamiltonian, *D* and *E* (−3.22 cm^{-1} to −3.44 cm^{-1} and −0.16 cm^{-1} to −0.21 cm cm^{-1}, respectively) and demonstrates a clear correlation between the degree of the structural distortion and the *E* parameter. The *ab-initio* CASSCF method was employed to calculate the zero-field splitting parameters. "Broken symmetry" density functional theory calculations were performed to estimate the magnitude of the Mn−Mn exchange interactions.

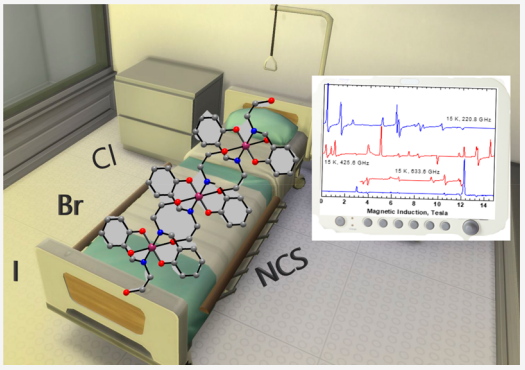

INTRODUCTION

The coordination chemistry of manganese(III) attracts persistent attention mainly for its principal role in the important catalytic cycles in nature.[1−3] In addition, a special interest in this subject has been caused by the discovery of single-molecule magnet (SMM) behavior in the mixed (III, IV) valence complex $[Mn_{12}O_{12}(O_2CCH_3)_{16}(H_2O)_4]$.[4] The electronic configuration of Mn(III) centers with $S = 2$ ground spin state $t_{2g}^3e_g^1$ and a strong axial magnetic anisotropy resulting from the Jahn−Teller effect make them potentially good candidates for demonstration of single molecule magnet (SMM),[5] single ion magnet (SIM),[6−9] and single chain magnets (SCM)[10−13] properties and, thus, for the creation of high information density storage materials. At the same time, the development of the Mn(III) chemistry has not been satisfactory because of the synthetic problems associated with Mn(III) disproportionation processes and the formation of insoluble and very stable MnO_2.[14] Herein, we report a simple and effective synthetic route to a series of cationic and molecular polymeric Mn(III) chain complexes $\{[Mn(HL^{1,2})_2]X\}_n$ (**1**−**7**) and $[Mn(HL^2)_2(NCS)]_n$ (**8**), (H_2L^1 = 2[(2-hydroxyethyl)iminomethyl]phenol, H_2L^2 = 2[(2-hydroxyethyl)iminomethyl]-6-methoxyphenol; X = Cl, Br, I, NCS) as well as a detailed investigation of the complexes by X-ray crystallography, Fourier transform infrared (FTIR) spectroscopy, and high-field electron paramagnetic resonance (HFEPR) methods, combined with density functional theory (DFT) calculations.

RESULTS AND DISCUSSION

Synthesis, Spectroscopic Analysis, and Crystal Structures of Manganese Complexes. The general synthetic route is depicted in Scheme 1. The Schiff base ligands H_2L^1 and H_2L^2 were prepared *in situ* by condensation of 2-

Received: August 30, 2019
Revised: January 16, 2020
Published: January 21, 2020

Scheme 1. Synthesis of Manganese Complexes 1−8

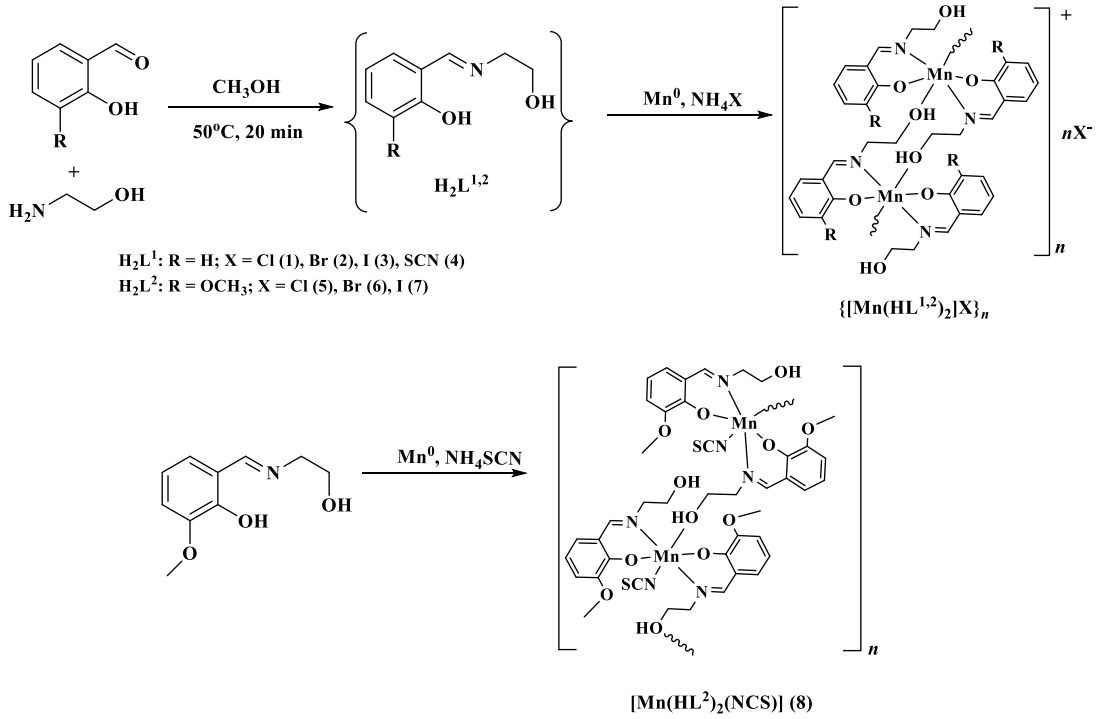

aminoethanol with salicylaldehyde or *o*-vanillin, respectively. Manganese complexes **1**−**8** were obtained via the "direct synthesis" (DS) approach, which is based on using regular metal powders instead of their salts as a source of metal. This method has been widely investigated by our group,[15,16] and it has been shown that in some cases there are advantages in exploiting DS conditions as compared to the traditional "wet" chemistry. For example, a better morphology of the crystal products and absence of contaminating anions were noticed. At the same time, there is a possibility to obtain complexes with the metals whose salts are very expensive or commercially unavailable as starting materials.[17,18] It should be noted that a synthesis of complex **1** by using metal salt as a precursor was previously reported.[19] All DS reactions were performed by heating and magnetic stirring in open air. Total dissolution of the metal powders indicated the reaction end. Crystals suitable for X-ray analysis were formed within few days when the resulting brown solutions were allowed to stand at room temperature. For the complexes $[Mn(HL^2)_2]Cl$ (**5**) and $[Mn(HL^2)_2]Br$ (**6**), the single crystals have not been obtained, and their composition was confirmed by elemental analysis, FTIR, and HFEPR methods. It is noteworthy that in the systems with an ammonium thiocyanate, two different complexes with the same composition $Mn(HL^{1,2})_2(NCS)$ but different crystal structure were obtained (Scheme 1).

The IR spectra of compounds **1**−**8** show similar absorption bands and confirm the presence of the Schiff base ligands. Very strong bands in the region 1599−1649 cm^{-1} were assigned to the double imino (C═N) bonds vibrations. The broad bands in the region 3400−3100 cm^{-1} indicate the presence of hydroxo groups, which are partially deprotonated in all complexes. Noncoordinated and coordinated thiocyanate anions in **4** and **8** are confirmed by the presence of the intense peaks (CN) at 2055 and 2071 cm^{-1} and weak (CS) vibrations at 760 and 784 cm^{-1}, in **4** and **8**, respectively.

X-ray crystal structures were determined for the compounds **2**−**4** and **8** (Table 6) and those for **1** and **7** have been reported earlier.[19,20] All complexes are one-dimensional (1D) polymers based on Mn(III) centers. The crystal lattices of the halogenide complexes are similar and consist of the cationic chains $[Mn(HL^{1,2})_2^+]_n$ (Figure 1) and counterions X^- (Cl, Br, I), while the thiocyanate complexes possess both cationic (**4**) and neutral chain (**8**) structures depending on the ligand used (Figures 2−3). In the case of compound **4**, packing of above-mentioned chains containing inversion centers and acentric SCN^- anions results in the chiral $P2_12_12_1$ space group.

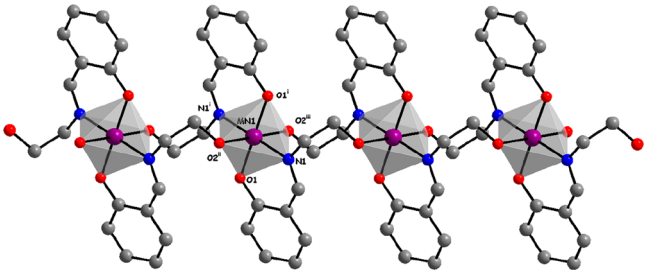

Figure 1. Crystal structure of the polymeric cation $[Mn(HL^{1,2})_2]_n^{n+}$ in **1**−**4** and **7**. Hydrogen atoms and methoxy groups are omitted. Symmetry operations: (i) $-x, -y, -z$; (ii) $x, 1 + y, z$; (iii) $-x, -1 - y, -z$.

The metal atoms are hexacoordinated with $[N_2O_4]$ or $[N_3O_3]$ environments typical for Mn(III) pseudo-octahedral (4 + 2) geometry. The deviation from ideal O_h symmetry relates mainly to linear parameters of the metal coordination polyhedra (the differences in the bond lengths being of more than 0.4 Å) and is negligible for angular parameters with maximal values observed for **8** (Table 1). The +3 manganese oxidation state is readily seen in the EPR spectra (see below), as signals of an $S = 2$ spin state are detected. This was also

https://dx.doi.org/10.1021/acs.cgd.9b01150
Cryst. Growth Des. 2020, 20, 1491−1502

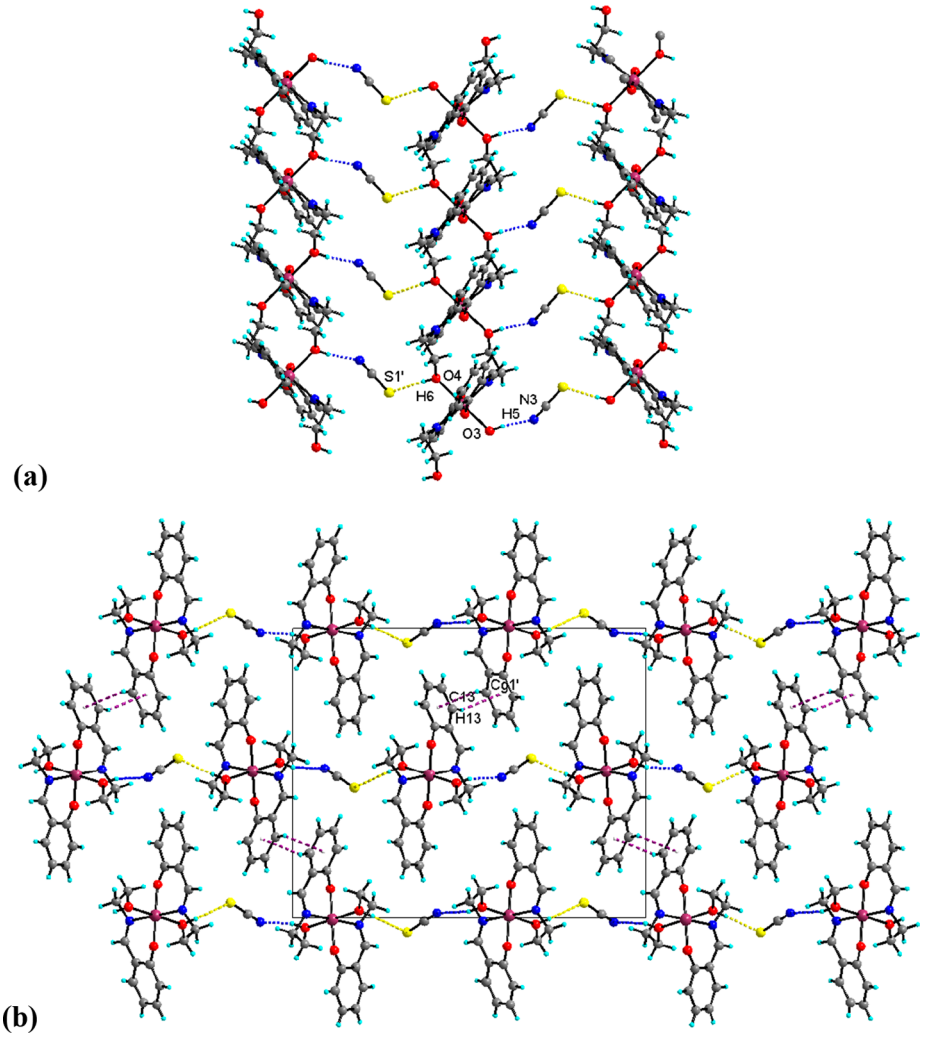

Figure 2. Crystal structure of **4**: (a) H-bonded layers; and (b) projection of crystal packing viewing along the [100] direction. Symmetry operations: (a) (i) 1.5 − *x*, 1 − *y*, 0.5 + *z*; (b) Cg1′ is a centroid of the C9···C14 benzene ring (i) 1 − *x*, 0.5 + *y*, 0.5 − *z*.

confirmed by comparison of coordination bond distances, existence of Jahn−Teller elongation, and bond valence sum calculation (Table 1).

The 1D polymeric structure is achieved due to chelate-bridging function of the ligands, $[2.01_1 1_1 1_2]$ by Harris notation.[23] The cationic chains along with bridging X anions located on inversion centers form H-bond based layers parallel to the *ab* plane which are further interconnected by C−H···π bonds between HL rings to yield a three-dimensional (3D) supramolecular architecture (Figure 4; Tables 2 and 3).

The maximum similarity of the crystal structure is observed for the halide complexes with H_2L^1 (**1**−**3**); nevertheless, they are not isostructural. There is a direct correlation between the size of the halogen atom and the intrachain Mn···Mn distance as increasing the radius of the ion halide in the sequence Cl(1.81 Å) < Br(1.97 Å) < I(2.23 Å)[24] leads to the interatomic distance increase by approximately 0.02 Å (Table 3). However, for the complex **4** with NCS, which is the largest anion in the sequence, the Mn···Mn distance is somewhat smaller than expected which can be explained by a different way of crystal packing with C−H···π interactions between the aromatic rings of H_2L^1 (Figure 2, Table 3).

The presence of a bulky methoxy group in the benzene ring of H_2L^2 has a noticeable effect on the packing of the iodide complex **7**, where the polymeric cations and iodide anions form a H-bonded chain supramolecular frame unlike the layer found in the halide complexes with H_2L^1 (Figure 5).

The most drastic differences are observed when replacing the SB ligand in the thiocyanate complex: instead of the cationic complex $[Mn(HL^1)_2]NCS$ **4**, a neutral complex of the analogous composition $[Mn(HL^2)_2(NCS)]$ **8** was obtained (Figure 3). In **8**, the $\{MnN_3O_3\}$ chromophore is formed by two monodeprotonated SB ligand molecules with different coordination modes (N,O-chelated and O,N,O′-bridging-chelate) and N-coordinated thiocyanate group. The metal atom shifted from the equatorial plane by ca. 0.07 Å toward N_{NCS}. The manganese atoms in $\{Mn\}_n$ chains are arranged in a zigzag fashion with a Mn···Mn distance of 6.7 Å and Mn−Mn−Mn angles of 121.3°.

Each noncoordinated S-donor atom from the NCS group forms two H-bonds with OH groups from aminoalcohol arms of the bridging SB ligand (intra-HB) and the chelate ligand (inter-HB) (Figure 3, Table 2).

High-Field EPR Spectra. The ground state of the Mn(III) ion is the even-spin $S = 2$ state, and complexes containing Mn(III) exhibit typically large zero-field splitting with the D parameter of the spin Hamiltonian (1) of a few cm^{-1}, making them very difficult to investigate by standard EPR, as the small

https://dx.doi.org/10.1021/acs.cgd.9b01150
Cryst. Growth Des. 2020, 20, 1491−1502

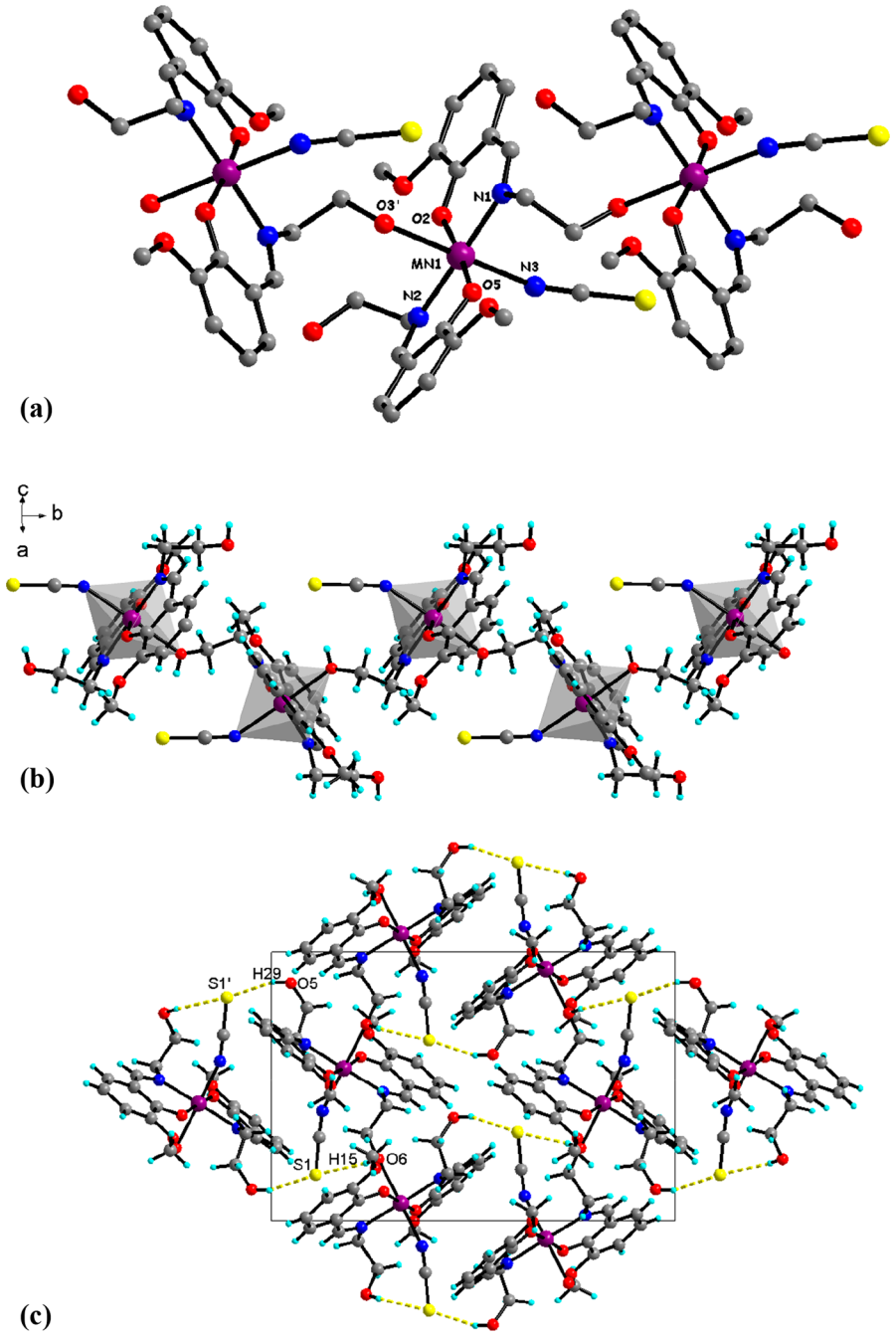

Figure 3. Crystal structure of **8**: (a) molecular structure with labeling scheme; (b) fragment of polymeric chain $[Mn(HL^2)_2(NCS)]_n$; and (c) projection of crystal packing viewing along the [010] direction. Symmetry operations: (a) (i) $1.5 - x, -0.5 + y, 1.5 - z$; (c) (i) $1 - x, 1 - y, 2 - z$.

microwave quantum energy cannot cause transitions between the M_S levels

$$\hat{\mathbf{H}} = \mu_B \mathbf{B}\{\mathbf{g}\}\hat{\mathbf{S}} + D\left\{\hat{\mathbf{S}}_z^2 - \frac{1}{3}S(S+1)\right\} + E(\hat{\mathbf{S}}_x^2 - \hat{\mathbf{S}}_y^2) + B_4^0\mathbf{O}_4^0 + B_4^4\mathbf{O}_4^4 \quad (1)$$

Interestingly, there is one exception to this: the $M_S = 2$ and $M_S = -2$ levels of the $S = 2$ state are split very little in the absence of the magnetic field (approximately $3E^2/D$), and a nominally "forbidden" $\Delta M_S = 4$ transition sometimes appears in X-band EPR at an effective g value of ~8.[2,25−29] The transition under question is however only weakly sensitive to the D parameter. HFEPR offers an effective remedy to these problems.[30−33] The microwave quantum energies available to us are up to ~20 cm^{-1} (~600 GHz) and allow observation of all possible transitions in Mn(III) systems. Complexes of Mn(III) tend to produce HFEPR spectra of good quality. Out of the eight complexes studied in this work, **1**, **2**, **4**, **5**, and **6** behaved very well, while the two iodide-containing species **3** and **7** as well as complex **8**, containing thiocyanate coordinated to Mn, posed problems (see below). Figure 6 shows spectra of **5** recorded at 15 K with various microwave frequencies.

To determine the spin Hamiltonian parameters accurately, a large number of spectra were recorded, and the resonance fields were plotted versus the microwave frequency (Figure 7 for complex **5**). The dependencies so obtained were fitted, resulting in the spin Hamiltonian parameters in Table 4.

https://dx.doi.org/10.1021/acs.cgd.9b01150
Cryst. Growth Des. 2020, 20, 1491−1502

Table 1. Comparison of Geometrical Parameters of the Mn Coordination Polyhedra in 1−4 and 8

	H_2L^1				H_2L^2	
	1[a]	2	3	4	7[a]	8
Mn−O (short), Å	1.866(2)	1.873(1)	1.871(1)	1.861(3)	1.829(8)	1.844(2)
				1.876(3)	1.849(8)	1.864(2)
Mn−O (long), Å	2.287(2)	2.287(2)	2.288(1)	2.242(3)	2.247(8)	2.340(2)
				2.282(3)	2.315(8)	
Mn−N, Å	2.023(2)	2.029(2)	2.026(2)	2.037(4)	2.040(1)	2.031(2)
				2.049(4)	2.061(9)	2.053(2)
						2.231(2)
Δ_{max}[b], Å	0.421(2)	0.414(2)	0.417(2)	0.421(4)	0.418(9)	0.496(2)
BVS[c]	3.05	3.00	3.02	3.01	3.08	3.13
trans-angles, deg	180	180	180	177.9(2)	179.0(4)	178.43(7)
				178.9(1)	179.2(5)	173.02(7)
				179.1(2)	179.5(5)	178.39(7)
Δ_{max}, deg	0	0	0	2.1(2)	1.0(5)	5.41(7)
cis-angles, deg	87.29(7)−92.71(7)	86.97(6)−93.03(6)	87.33(5)−92.67(5)	87.5(1)−93.6(1)	86.8(3)−92.5(4)	84.78(6)−93.89(7)
Δ_{max}, deg	5.42(7)	6.06(6)	5.34(5)	6.1(1)	5.7(4)	9.11(7)

[a]The crystallographic data for **1** and **7** were previously reported in refs 19 and 20, respectively. [b]Δmax − the difference between a maximal and a minimal bond length or angle. [c]BVS − bond valence sum for Mn atoms.[21,22]

Taking into account the quartic parameters of spin Hamiltonian (1), B_0^4 and B_4^4 had a very small effect on the fit quality and on other parameters.

An additional advantage of HFEPR is the easy D sign determination. The positions of the EPR transitions do not depend on the sign of D or E in eq 1, but spectra taken at low temperatures exhibit an intensity pattern depending on the sign, resulting in complete freezing out of certain transitions, as shown in Figure 8. This effect depends on the magnitude of the Zeeman energy rather than on the D magnitude, and the sign of a small D can also be determined.[34−36]

Complex **8** differs from other ones by having an SCN^- anion coordinated to Mn; it is thus interesting to compare its spin Hamiltonian parameters to those of the remaining compounds in which the anions are noncoordinated. Unlikely most other systems (except for **7**), difficulties were encountered in recording the EPR spectra of **8**. The compressed powder samples exhibited too many features, which could not be explained within the monomeric Mn^{3+} model (Figure S4). These features were also present when using eicosane pellets with dispersed powder of **8**, thus eliminating the possibility that they were due to magnetic torquing. A subset of resonances could be found whose frequency dependencies allowed us to determine the parameters of **8** in Table 4. Other spectral features may be due to weak interactions between the Mn(III) ions. The D value in **8** was the largest in the series, but the differences along the series were not dramatic. The D parameter ranges from −3.197 to −3.44 cm^{-1} (Table 4), which is just a 7% change. The E parameter shows a larger relative variation, from −0.525 in **3** to −0.77 cm^{-1} in **8**. The E parameter tends to be larger in the H_2L^2 ligand complexes, in agreement with the generally more distorted structures compared to those of H_2L^1 ligand.

Calculations of the Zero-Field Splitting. The zero-field splitting (zfs) is a result of spin-orbit coupling and ligand field splitting of energy levels of a paramagnetic atom possessing spin larger than 1/2. Dependencies between the zfs parameters and the ligand-field energies for various electronic configurations are well-known.[37−39] The ^5D term of the Mn(III) ion in an elongated tetragonal bipyramid gives rise to a $^5B_{1g}$ ground state and the D parameter is usually negative, with rare exceptions.[40,41] The excited states contributing to the zero-field splitting via the spin-orbit coupling are ^5E_g and $^5B_{1g}$ states, derived from ^5D free-ion term, and the ^3E_g state derived from the ^3H term. The ligand-field splittings, which are needed to relate the spin Hamiltonian parameters to the electronic spectra, are typically difficult to obtain due to the presence of intense $\pi-\pi^*$ and charge transfer bands. In more recent years, density functional theory (DFT) and *ab initio* methods have been applied to get insight into the nature of the zero-field splitting.[41−43] It is now believed that the contribution of the spin−spin interactions to the zero-field splitting is not necessarily negligible compared to the spin−orbit coupling contribution. We have attempted to calculate the spin−orbit coupling contribution to D and E in our complexes using the state-averaged complete active space self-consistent field (CASSCF)[41−43] approach, with four electrons in five orbitals. Five quintet and lowest 35 triplet states were taken into account, such as in refs 41−43. Functional B3LYP was employed with TZVPP functions for Mn and all coordinated atoms and SVP functions for all remaining atoms.[44−46] Calculations were performed using the ORCA software package.[47] The spin−spin contribution was calculated using the "coupled-perturbed" scheme as implemented in ORCA (see also refs 41−43). A single molecule was cut out of the chain of each compound presented in Table 6 by inserting hydrogen atoms at appropriate positions. These entities bear charge +1 for all species except **8**, which is neutral. The noncoordinated anions were not used, but for **1** calculations were performed both for a $\mathbf{1}^+$ cation and a $\mathbf{1}^-$ anion in which two Cl^- ions closest to Mn were taken into account. The differences in the calculated zero-field splitting parameters were minuscule (Table 5). It is interesting to compare species **4** to **8**, because **8** has a coordinated SCN^- ion, while in **4** SCN^- is not coordinated, like anions in all other molecules. For **4**, D = −3.432 cm^{-1}, and E = −0.528 cm^{-1} were obtained. The D and E found in this way compare well to the experimental values in Table 4. The spin−spin contributions to D and E were −0.453 cm^{-1} and −0.046 cm^{-1}, respectively, while the spin−orbit coupling related contribution was −2.978 cm^{-1} and −0.482 cm^{-1}, respectively. The direction of the largest component (D_{zz}) of the calculated D tensor was found

https://dx.doi.org/10.1021/acs.cgd.9b01150
Cryst. Growth Des. 2020, 20, 1491−1502

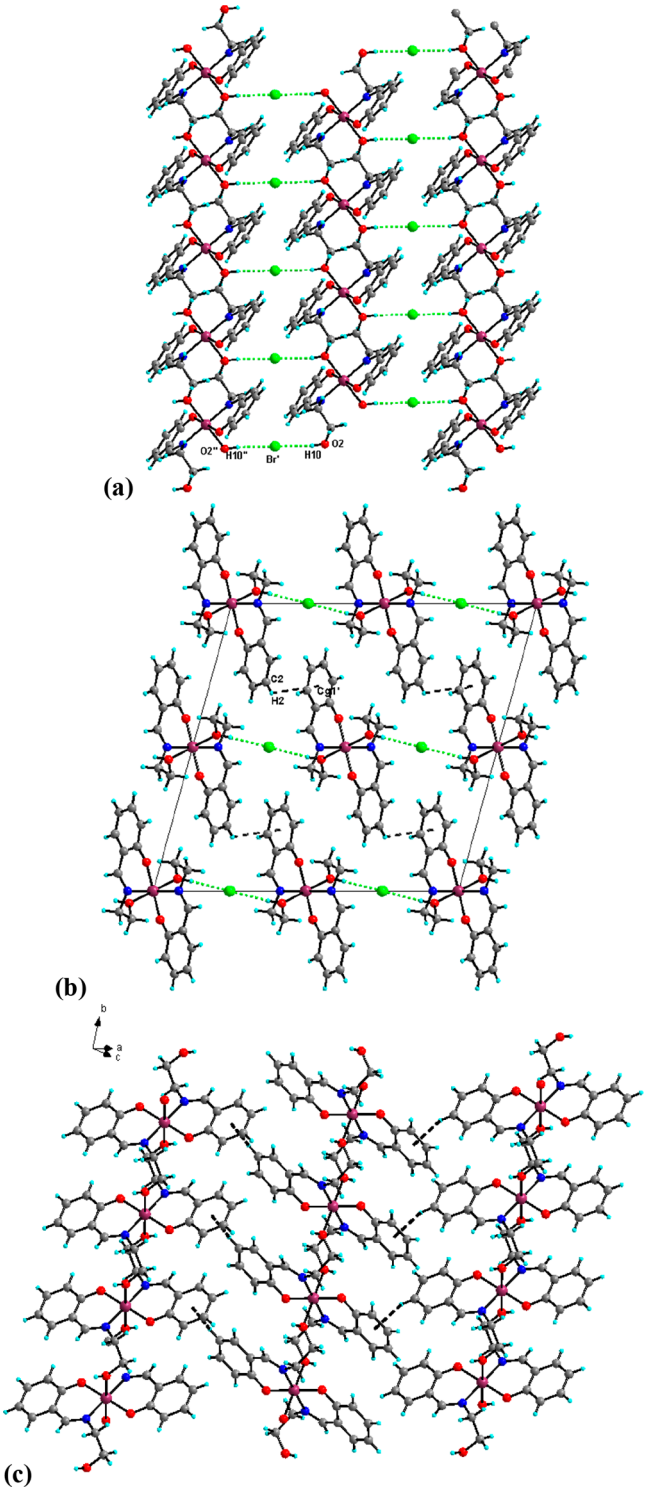

Figure 4. Crystal structure of **2**: (a) H-bonded layers; (b) projection of crystal packing viewing along the [010] direction; (c) layers based on C−H···π bonds. Symmetry operations: (a) (i) $-x, -1+y, 0.5-z$; (ii) $-0.5-x, -1.5-y, -z$; (b) Cg1′ is a centroid of the C1···C6 benzene ring (i) $x, 1-y, -0.5+z$.

3.0 deg away from the long Mn−$O_{alcohol}$ bond, or 1.9 deg away from the normal to the least-squares NNOO plane of the Schiff base donor atoms. For **8**, the calculations produced $D = -3.507$ cm^{-1}, $E = -0.578$ cm^{-1}. The spin−orbit contributions to D and E were -3.064 cm^{-1} and -0.536 cm^{-1}, respectively, while the spin−spin contributions were -0.443 cm^{-1} and -0.042 cm^{-1}. The replacement of an alcoholato ligand by SCN^- thus does not cause the magnitude of D to change much. The calculated D_{zz} direction in **8** was found 1.7 deg away from the Mn−$N_{thiocyanate}$ bond, or 3.2 deg from the Mn−$O_{alcohol}$ bond (Figure 9). The calculations, while reproducing well the experimental D magnitudes, fail to reproduce the substantially increased experimental E for **8** compared to **4**. Similar calculations, the results of which are presented in Table 5, show a narrow range of slightly overestimated D and slightly underestimated E values.

Table 2. Hydrogen Bonds Parameters in 1−4, 7, 8[a]

D−H···A	H···A	D···A	D−H···A
	1		
O2−H10···Cl	2.299(1)	3.057(2)	164(2)
	2		
O2−H10···Br1′	2.42(1)	3.265(2)	173(3)
	3		
O2−H5···I1′	2.66(1)	3.508(1)	172(3)
	4		
O3−H5···N3	1.88(4)	2.706(5)	162(8)
O4′−H6′···S1	2.31(6)	3.154(3)	175(9)
	7		
O5″−H5″···I1A	2.863(1)	3.488(8)	131(6)
O6′−H6′−I1B	2.620(4)	3.477(9)	173(6)
	8		
O5−H29···S1′	2.66(3)	3.426(2)	155(3)
O6′−H15′···S1′	2.60(3)	3.347(2)	167(3)

[a]Symmetry transformations used to generate equivalent atoms: (**2**) (i) $-x, -1+y, 0.5-z$; (**3**) (i) $-0.5+x, -0.5+y, z$. (**4**) (i) $1.5-x, 1-y, 0.5+z$ (**7**) (i) $x, 1+y, z$, (ii) $-x, 1-y, 0.5+z$; (**8**) (i) $1-x, 1-y, 2-z$.

Mn−Mn Interactions. The EPR spectra obtained in this work were in general of good quality, but were not as good as those previously obtained in this lab for some other Mn(III) systems.[30,48,49] The reason for this may be the interactions between the Mn(III) ions. The bridges between the manganese ions are not likely to transmit significant exchange interactions. A fragment containing two Mn ions was cut out of the chain of **4**, and a broken-symmetry calculation[50−53] was performed. Similarly as in the calculations of D above, the ORCA software was employed using functional B3LYP with TZVPP functions for Mn and all coordinated atoms and SVP functions for all remaining atoms. The structures used for the broken-symmetry calculations are shown in the Supporting Information. An exchange integral value J of just 0.02 cm^{-1} (antiferromagnetic, using the Heisenberg−Dirac−Van Vleck Hamiltonian in a form $\mathbf{H} = J\mathbf{S}_1\mathbf{S}_2$) was obtained. The same value is obtained when calculating exchange interactions through the hydrogen bridges involving the SCN^- ion in **4**. For **8**, $J = 0.04$ cm^{-1} was calculated, although the Mn−Mn distance in the chain of 6.695 Å was larger than in **4** (5.725 Å). It should be mentioned here that the magnitude of the exchange interactions depends less on the interatomic distance than on the nature of a bridge between the metal atoms. For example, a 2 orders of magnitude larger J of 2.9 cm^{-1} (translated to the notation used in this paper) was found in a Mn(III) dimer with a slightly shorter Mn−Mn distance than in our complexes, in which exchange is transmitted by a system of π bonds.[54] We performed a broken symmetry calculation using the published structure to obtain J of 2.5 cm^{-1}, in good agreement with experiments. It is noteworthy here that the

https://dx.doi.org/10.1021/acs.cgd.9b01150
Cryst. Growth Des. 2020, 20, 1491−1502

Table 3. Selected C−H···π Interactions and Mn···Mn Distances in 1−4 and 7 and 8

	H_2L^1				H_2L^2	
	1(Cl)	2 (Br)	3 (I)	4 (NCS)	7 (I)	8 (NCS)
C−H···π, Å	2.806(1)	3.2020(2)	3.3206(1)	2.5930(1)	3.4252(3)	
Mn···Mn, Å	5.700(2)	5.7196(3)	5.7552(2)	5.7247(9)	5.898(4)	6.6950(4)

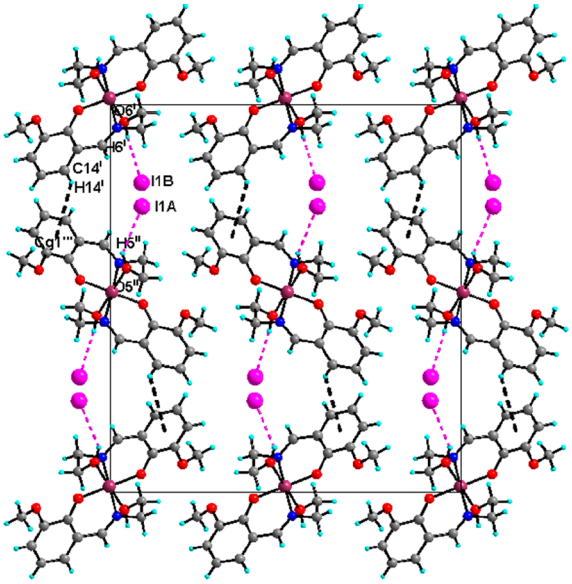

Figure 5. Projection of crystal packing of 7 viewing along the [010] direction. Symmetry operations: (i) x, 1 + y, z, (ii) −x, 1 − y, 0.5 + z; Cg1′ is a centroid of the C1···C6 benzene ring (iii) 0.5 − x, −2 + y, −0.5 + z.

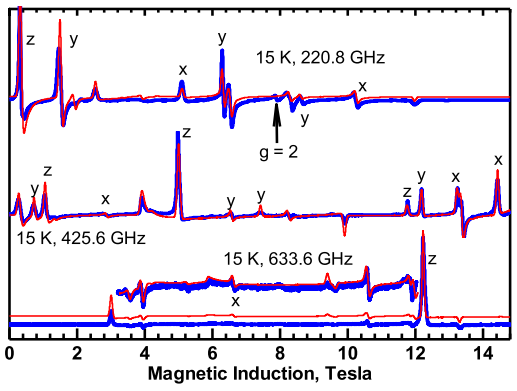

Figure 6. EPR spectra of 5 recorded at conditions indicated. Blue: experimental; red: simulated using parameters from Table 4. Labels x, y, and z indicate the molecular orientation at which a transition occurs. The unlabeled features correspond to the off-axial turning points.

EPR spectra of 8 (Figure S4) exhibit the most visible evidence of the metal−metal interactions in this series, in the form of additional splittings observed on some resonances. Exchange interactions of this order of magnitude are indeed sufficient to split the EPR resonances in some Mn(III) dimers,[55] while they are not detectable in magnetic susceptibility measurements. The Mn−Mn distances in chains which are of the order of 5.7 Å give rise to the dipole−dipole interactions of some −0.03 cm^{-1}, comparable to the exchange interactions estimated above. Both dipolar and exchange effects are likely to affect the EPR linewidth and may create additional spectral features. The

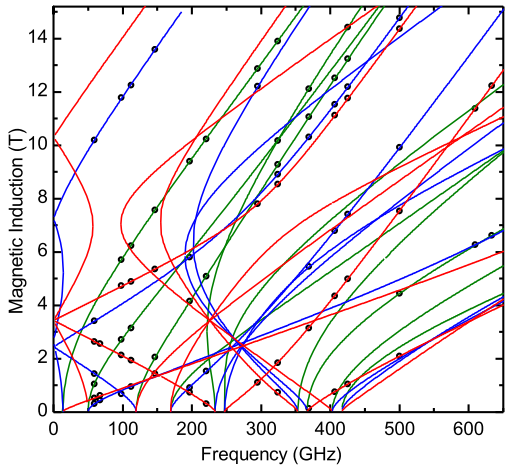

Figure 7. Frequency dependencies of the resonance fields corresponding to the canonical transitions in 5. Circles: experimental resonance positions; green, blue and red lines: calculated X, Y, and Z resonances, respectively. The lines with the highest slope represent the "allowed" ΔM_S = 1 transitions. The plots of the "forbidden" transitions (ΔM_S > 1) have lower slopes.

metal−metal interactions in 8 occur in extended systems, unlike the discrete dimers studied in ref 55, and the problem seems impossible to be solved without using single-crystal EPR spectra.

EXPERIMENTAL SECTION

General Procedures. Reactions were carried out under air and using HPLC solvents. The IR spectra were done on ATR Bruker Vertex 70 spectrophotometer in the 4000−400 cm^{-1} range. Elemental analyses were recorded using Flash 2000 Fisher Scientific Thermo Electron analyzer.

EPR. The HFEPR spectra at temperatures ranging from ca. 3 to 290 K were recorded on a home-built spectrometer at the EMR facility of the NHMFL.[56] The instrument is equipped with a superconducting magnet (Oxford Instruments) capable of reaching a field of 17 T. Microwave frequencies over the range 52−630 GHz were generated by a phase-locked Virginia Diodes source, producing a base frequency of 13 ± 1 GHz, which was multiplied by a cascade of frequency multipliers. The instrument is a transmission-type device and uses no resonance cavity.

Syntheses. *{[Mn(HL^1)$_2$]Cl}$_n$ (1).* 2-Aminoethanol (0.36 mL, 6 mmol) and salicylaldehyde (0.56 g, 6 mmol) were added to 30 mL of methanol and stirred magnetically for 15 min until the color of the solution turned in yellow. After manganese powder (0.11 g, 2 mmol) and NH_4Cl (0.21 g, 4 mmol) were added to the solution, the reaction mixture was stirred at 50 °C for ca. 2 h. Total dissolution of manganese powder was observed. The dark brown crystals were collected after 1 day by filtration, washed with isopropanol, and dried in air; yield 330 mg (39%, per Mn). The elemental analysis for $C_{18}H_{20}N_2O_4ClMn$ (M_r = 418.76). Calcd: C, 51.63; H, 4.81; N, 6.69; Mn, 13.12%. Found: C, 51.55; H, 4.74; N, 6.55; Mn, 13.00%. IR (ATR, cm^{-1}): 3155 (br), 2924 (w), 1612 (s), 1550 (s), 1441 (s), 1304 (s), 1218 (s), 1025 (m), 885 (m), 769 (s), 634 (m), 457 (s).

A different method of synthesis using manganese chloride tetrahydrate was reported previously.[19]

https://dx.doi.org/10.1021/acs.cgd.9b01150
Cryst. Growth Des. 2020, 20, 1491−1502

Table 4. Experimental Spin Hamiltonian Parameters[a]

complex	g_x	g_y	g_z	D (cm^{-1})	E (cm^{-1})	B_4^0 (cm^{-1})	B_4^4 (cm^{-1})
1[b] (H_2L^a)	1.982(4)	1.985(4)	1.998(2)	−3.231(2)	−0.578(2)	0	−0.002(1)
2 (H_2L^a)	1.980(2)	1.974(2)	1.988(3)	−3.223(3)	−0.548(2)	−0.0006(1)	0.003(1)
3 (H_2L^a)	1.984(4)	1.963(3)	1.998(5)	−3.197(3)	−0.525(3)		0
4 (H_2L^a)	1.998(1)	1.986(1)	1.992(2)	−3.296(3)	−0.662(2)	−0.0003(1)	−0.0019(1)
5 (H_2L^b)	2.001(2)	1.997(1)	1.998(2)	−3.271(2)	−0.663(1)	−0.0001(1)	−0.0034(5)
6 (H_2L^b)	1.999(1)	1.997(1)	2.000(1)	−3.290(2)	−0.699(2)	−0.0003(1)	−0.0006(3)
7 (H_2L^b)	1.999(9)	1.961(4)	1.990(6)	−3.34(1)	−0.76(1)	0	0
8 (H_2L^b)	2.00 (1)	1.97(1)	1.96 (1)	−3.44(1)	−0.77(1)	0	0

[a]Zero values of B_4^0 and B_4^4 indicate that they have not been fitted. [b]A one-year old sample of **1** exhibited slightly altered spin Hamiltonian parameters (see Figure S1).

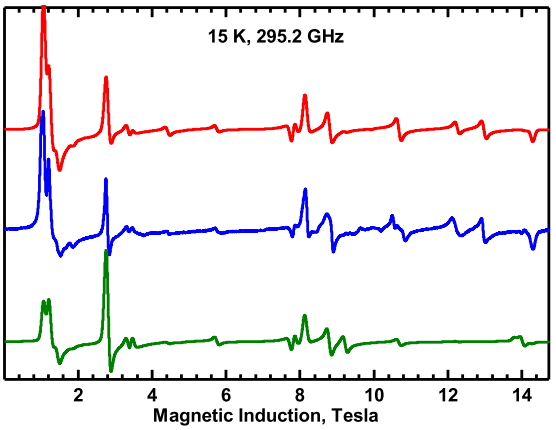

Figure 8. HFEPR spectrum of **4**. Blue: experimental; red: simulated using parameters from Table 4; green: simulated with the signs of D and E inverted.

{[Mn(HL^1)$_2$]Br}$_n$ (**2**). This complex was prepared in a way similar to that of **1**, but using NH_4Br (0.39 g, 4 mmol) instead of NH_4Cl. The dark brown crystals were collected after 1 day by filtration, washed with isopropanol, and dried in air; yield 320 mg (35%, per Mn). The elemental analysis for $C_{18}H_{20}N_2O_4BrMn$ (M_r = 463.20). Calcd: C, 46.67; H, 4.35; N, 6.05; Mn, 11.86%. Found: C, 46.54; H, 4.14; N, 5.85; Mn, 11.50%. IR (ATR, cm^{-1}): 3151 (br), 2929 (w), 1607 (vs), 1546 (s), 1445 (s), 1300 (s), 1215 (s), 1025 (m), 884 (m), 767 (s), 638 (m), 456 (s).

{[Mn(HL^1)$_2$]I}$_n$ (**3**). This complex was prepared in a way similar to that of **1**, but using NH_4I (0.58 g, 4 mmol) instead of NH_4Cl. The dark brown crystals were collected after 1 day by filtration, washed with isopropanol, and dried in air; yield 410 mg (40%, per Mn). The elemental analysis for $C_{18}H_{20}N_2O_4IMn$ (M_r = 510.20). Calcd: C, 42.37; H, 3.95; N, 5.49; Mn, 10.77%. Found: C, 42.15; H, 3.83; N, 5.24; Mn, 10.46%. IR (ATR, cm^{-1}): 3149 (br), 2915 (w), 1607 (vs), 1544 (s), 1439 (s), 1305 (s), 1218 (s), 1030 (m), 890 (m), 760 (m), 640 (m), 449 (s).

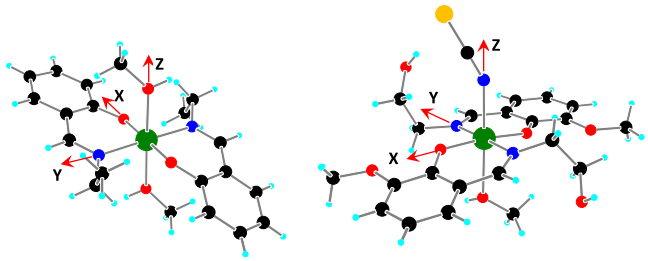

Figure 9. Structures of **4** (left) and **8** (right) used for the ORCA calculations and the D tensor axes directions resulting from calculations.

{[Mn(HL^1)$_2$]NCS}$_n$ (**4**). This complex was prepared in a way similar to that of **1**, but using NH_4NCS (0.31 g, 4 mmol) instead of NH_4Cl. The dark brown crystals were collected after 1 day by filtration, washed with isopropanol, and dried in air; yield 220 mg (25%, per Mn). The elemental analysis for $C_{19}H_{20}N_3O_4SMn$ (M_r = 441.38). Calcd: C, 51.70; H, 4.57; N, 9.52; S, 7.26; Mn, 12.44%. Found: C, 51.65; H, 4.28; N, 9.36; S, 7.15; Mn, 12.25%. IR (ATR, cm^{-1}): 3145 (br), 3056 (w), 2924 (w), 2071 (s), 1599 (vs), 1543 (s), 1444 (s), 1293 (m), 1219 (m), 1025 (m), 885 (m), 757 (s), 683 (m), 456 (s).

{[Mn(HL^2)$_2$]Cl}$_n$ (**5**). This complex was prepared in a way similar to that of **1**, but using *o*-vanillin (0.94 g, 6 mmol) instead of salicylaldehyde. The dark brown precipitate was collected after 1 day by filtration, washed with isopropanol, and dried in air; yield 212 mg (43%, per Mn). The elemental analysis for $C_{20}H_{24}N_2O_6ClMn$ (M_r = 487.81). Calcd: C, 50.17; H, 5.05; N, 5.85; Mn, 11.47%. Found: C, 50.05; H, 4.97; N, 5.74; Mn, 11.35%. IR (ATR, cm^{-1}): 3434(br), 3396 (w), 3186 (br), 2936 (w), 1607 (vs), 1551 (m), 1469 (s), 1300 (m), 1249 (s), 1029 (m), 864 (s), 744 (s), 640 (m), 453 (m).

It should be noted that **5** can be also obtained by the ordinary method of synthesis using manganese chloride tetrahydrate instead of manganese powder and ammonium chloride.

{[Mn(HL^2)$_2$]Br}$_n$ (**6**). This complex was prepared in a way similar to that of **5**, but using NH_4Br (0.39 g, 4 mmol) instead of NH_4Cl. The dark brown precipitate was collected after 1 day by filtration, washed with isopropanol, and dried in air; yield 320 mg (31%, per Mn). The elemental analysis for $C_{20}H_{24}N_2O_6BrMn$ (M_r = 523.26). Calcd: C,

Table 5. Experimental and Calculated Zero-Field Splitting Parameters

complex	D_{exp}, cm^{-1}	E_{exp}/D_{exp}	D_{calc}, cm^{-1}	E_{calc}/D_{calc}	D_{SO}[a], cm^{-1}	E_{SO}[a], cm^{-1}	D_{SS}[b], cm^{-1}	E_{SS}[b], cm^{-1}
1	−3.231	0.18	−3.464	0.13	−3.006	−0.457	−0.458	−0.036
1 + $2Cl^-$			−3.517	0.14	−3.065	−0.444	−0.452	−0.040
2	−3.223	0.17	−3.419	0.13	−2.958	−0.393	−0.461	−0.038
3	−3.197	0.16	−3.453	0.13	−2.991	−0.401	−0.462	−0.039
4	−3.296	0.20	−3.431	0.15	−2.978	−0.482	−0.453	−0.046
5	−3.271	0.20	−3.458	0.16	−3.005	−0.493	−0.453	−0.046
8	−3.44	0.21	−3.507	0.18	−3.064	−0.576	−0.443	−0.042

[a]Spin−orbit coupling contribution. [b]Spin−spin contribution.

https://dx.doi.org/10.1021/acs.cgd.9b01150
Cryst. Growth Des. 2020, 20, 1491−1502

Table 6. Crystallographic Data, Details of Data Collection, and Structure Refinement Parameters

	2	3	4	8
formula	$C_{18}H_{20}N_2O_4BrMn$	$C_{18}H_{20}N_2O_4IMn$	$C_{19}H_{20}N_3O_4SMn$	$C_{22}H_{26}N_4O_6S_2Mn$
M [g·mol^{-1}]	463.20	510.20	441.38	561.53
T [K]	150.00(10)	150.01(10)	150.00(10)	150.00(10)
crystal system	monoclinic	monoclinic	orthorhombic	monoclinic
space group	$C2/c$	$C2/c$	$P2_12_12_1$	$C2/c$
a [Å]	18.5786(9)	19.3631(5)	5.7247(3)	20.7615(7)
b [Å]	5.7196(3)	5.7552(2)	16.7646(7)	7.8546(3)
c [Å]	18.1494(10)	17.9767(5)	20.4425(8)	15.8834(5)
α [°]	90	90	90	90
β [°]	105.278(5)	102.470(3)	90	99.069(3)
γ [°]	90	90	90	90
V [Å^3]	1860.44(17)	1956.04(10)	1961.91(15)	2557.78(15)
Z	4	4	4	4
ρ_{calcd} [g·cm^{-3}]	1.654	1.732	1.494	1.458
μ [mm^{-1}]	8.513	18.096	6.733	6.107
goodness-of-fit on F^2	1.043	1.036	1.087	1.035
$F(000)$	936	1008	912	1164
$\theta_{min}/\theta_{max}$, (deg)	4.935/72.279	4.678/72.593	3.409/72.241	4.313/72.575
final R_1/wR_2 [$I > 2\sigma(I)$]	0.0256/0.0641	0.0192/0.0469	0.0373/0.0918	0.0391/0.1052
R_1/wR_2 (all data)	0.0303/0.0672	0.0207/0.0477	0.0408/0.1003	0.0440/0.1112
largest diff peak and hole (e Å^{-3})	0.346/−0.244	0.379/−0.422	0.304/−0.394	0.610/−0.363

45.91; H, 4.62; N, 5.35; Mn, 10.50%. Found: C, 45.75; H, 4.52; N, 5.27; Mn, 10.35%. IR (ATR, cm^{-1}): 3437 (br), 3393 (w), 3184 (br), 2931 (w), 1610 (vs), 1548 (m), 1473 (s), 1315 (m), 1239 (s), 1019 (m), 867 (s), 746 (s), 645 (m), 455 (m).

*{[Mn(HL^2)$_2$]I}$_n$ (**7**).* The synthesis of the complex **7** was previously reported by our group.[20]

*[Mn(HL^2)$_2$(NCS)] (**8**).* This complex was prepared in a way similar to that of **1**, but using *o*-vanilin (0.94 g, 6 mmol) instead of salicylaldehyde and NH_4NCS (0.31 g, 4 mmol) instead of NH_4Cl. Yellow crystals were collected after 1 day by filtration, washed with isopropanol, and dried in air; yield 300 mg (30%, per Mn). The elemental analysis for $C_{21}H_{24}N_3O_6SMn$ (M_r = 501.43). Calcd: C, 50.30; H, 4.82; N, 8.38; S, 6.39; Mn, 10.96%. Found: C, 50.16; H, 4.64; N, 7.98; S, 6.12; Mn, 11.30%. FT-IR (KBr, ν_{max} cm^{-1}): 3420 (br), 2919 (w), 2071 (vs), 1616 (vs), 1553 (m), 1475 (s), 1452(s), 1399 (m), 1353(w), 1303 (vs), 1227(s), 1193(m), 1112 (w), 1086(m), 1055(m), 1024(m), 979 (m), 902 (w), 864 (s), 784 (w), 742(s), 639(s), 590(w), 528(w), 471(w).

X-ray Structure Determination. Single crystal X-ray diffraction data were collected on an Agilent Technologies SuperNova diffractometer equipped with AtlasCCD detector and microfocus Cu-Kα radiation (λ = 1.54184 Å). The structures were solved by direct methods and refined on F^2 by full matrix least-squares techniques using SHELX97 (G.M. Sheldrick, 1998) package. All non-H atoms were refined anisotropically, and multiscan empirical absorption was applied using CrysAlisPro program (CrysAlisPro, AgilentTechnologies, V1.171.38.41r, 2015). The hydrogen atoms were included in the geometrically calculated position and refined riding on the corresponding atom. A summary of the crystallographic data and the structure refinement is given in Table 6. CCDC 1842146 (**2**), 1842148 (**3**), 1842149 (**4**), and 1854314 (**8**) contain the supplementary crystallographic data for this paper. This data can be obtained free of charge from The Cambridge Crystallographic Data Centre via www.ccdc.cam.ac.uk/data_request/cif.

CONCLUSIONS

A series of chain polymeric complexes with the general formula $Mn^{III}(HL)_2X$, where H_2L ligands are Schiff bases derived from salicylaldehyde or *o*-vanillin and 2-aminoethanol and X are Cl, Br, I and NCS, were prepared via a simple and productive "direct synthesis" approach based on a one-pot reaction between manganese powder, ammonium salt, and organic ligand formed *in situ* in methanol solution. X-ray analysis revealed two types of chain polymeric crystal structure for the obtained complexes: (1) the cationic chain structure consisting of the polymer cations $[Mn(HL^{1,2})_2]_n^+$ and counterions X^-, in compounds **1**−**7**, and (2) the molecular chain structure built of neutral polymeric molecules $[Mn(HL^2)_2(NCS)]_n$, in **8**. The metal centers inside the cationic chain are bridged through two {−NCCO−} fragments with a linear $\{Mn\}_n$ arrangement, while in the molecular chain they are linked with one NCCO-bridge forming the zig-zag metal atom arrangement. HFEPR spectroscopy was used to determine accurately the zero-field splitting parameters and was supported by DFT calculations. The data obtained are correlated with crystallographic results and demonstrate that the generally more distorted structures in compounds of ligand H_2L^2 compared to H_2L^1 give rise to larger E parameters in the former. The DFT calculations suggest the presence of very weak antiferromagnetic exchange interactions between Mn ions, which are stronger in complex **8** (0.04 cm^{-1}), containing coordinated SCN^- anions, than in other compounds (such as J = 0.02 cm^{-1} in **4**). They are presumably transmitted by the hydrogen bonds and seem to affect the HFEPR spectra of **8**, but they cannot make our compounds single chain magnets because of their expected antiferromagnetic character.

ASSOCIATED CONTENT

Supporting Information

The Supporting Information is available free of charge at https://pubs.acs.org/doi/10.1021/acs.cgd.9b01150.

HFEPR spectra of **1**−**3**, and **5**−**8**, the arrangements of the Mn moieties used to calculate the exchange integrals in **4** and **8** (PDF)

Accession Codes

CCDC 1842146, 1842148, 1842149, and 1854314 contain the supplementary crystallographic data for this paper. These data can be obtained free of charge via www.ccdc.cam.ac.uk/

https://dx.doi.org/10.1021/acs.cgd.9b01150
Cryst. Growth Des. 2020, 20, 1491−1502

data_request/cif, or by emailing data_request@ccdc.cam.ac.uk, or by contacting The Cambridge Crystallographic Data Centre, 12 Union Road, Cambridge CB2 1EZ, UK; fax: +44 1223 336033.

AUTHOR INFORMATION

Corresponding Authors

Svitlana Petrusenko − *Department of Inorganic Chemistry, Taras Shevchenko National University of Kyiv, Kyiv 01601, Ukraine;* orcid.org/0000-0001-8594-2643; Email: spetrusenko@yahoo.com

Andrew Ozarowski − *National High Magnetic Field Laboratory, Florida State University, Tallahassee, Florida 32310, United States;* orcid.org/0000-0001-6225-9796; Email: ozarowsk@magnet.fsu.edu; Fax: +1 850-644-1366

Authors

Oleh Stetsiuk − *MOLTECH-Anjou, UMR 6200, CNRS, UNIV Angers, 49045 Angers Cedex, France*

Nataliya Plyuta − *MOLTECH-Anjou, UMR 6200, CNRS, UNIV Angers, 49045 Angers Cedex, France; Department of Inorganic Chemistry, Taras Shevchenko National University of Kyiv, Kyiv 01601, Ukraine*

Narcis Avarvari − *MOLTECH-Anjou, UMR 6200, CNRS, UNIV Angers, 49045 Angers Cedex, France;* orcid.org/0000-0001-9970-4494

Evgeny Goreshnik − *Department of Inorganic Chemistry and Technology, Jožef Stefan Institute, 1000 Ljubljana, Slovenia*

Vladimir Kokozay − *Department of Inorganic Chemistry, Taras Shevchenko National University of Kyiv, Kyiv 01601, Ukraine*

Complete contact information is available at: https://pubs.acs.org/10.1021/acs.cgd.9b01150

Notes

The authors declare no competing financial interest.

ACKNOWLEDGMENTS

This work was supported in France by the CNRS, the University of Angers, the French Embassy in Kiev (grants to O.S. and N.P.) and the Ministry of Education and Science of Ukraine (Project No. 19BF037-05). The high-field EPR spectra were recorded at the NHMFL, which is funded by the NSF through the Cooperative Agreement No. DMR-1644779 and the State of Florida. E.G. gratefully acknowledges the Slovenian Research Agency (ARRS) for the financial support of the present study within the research program P1-0045 Inorganic Chemistry and Technology.

REFERENCES

(1) Rutherford, A. W.; Boussac, A. Water Photolysis in Biology. *Science* **2004**, *303*, 1782−1784.

(2) Gupta, R.; Taguchi, T.; Lassalle-Kaiser, B.; Bominaar, E. L.; Yano, J.; Hendrich, M. P.; Borovik, A. S. High-Spin Mn-Oxo Complexes And Their Relevance to the Oxygen-Evolving Complex Within Photosystem II. *Proc. Natl. Acad. Sci. U. S. A.* **2015**, *112*, 5319−5324.

(3) Tao, L.; Stich, T. A.; Soldatova, A. V.; Tebo, B. M.; Spiro, T. G.; Casey, W. H.; Britt, R. D. Mn(III) Species Formed by the Multi-Copper Oxidase MnxG Investigated by Electron Paramagnetic Resonance Spectroscopy. *JBIC, J. Biol. Inorg. Chem.* **2018**, *23*, 1093−1104.

(4) Sessoli, R.; Gatteschi, D.; Caneschi, A.; Novak, M. A. Magnetic bistability in a metal-ion cluster. *Nature* **1993**, *365*, 141−143.

(5) Boskovic, C.; Bircher, R.; Tregenna-Piggott, P. L. W.; Gudel, H. U.; Paulsen, C.; Wernsdorfer, W.; Barra, A.-L.; Khatsko, E.; Neels, A.; Stoeckli-Evans, H. Ferromagnetic and Antiferromagnetic Intermolecular Interactions in a New Family of Mn4 Complexes with an Energy Barrier to Magnetization Reversal. *J. Am. Chem. Soc.* **2003**, *125*, 14046−14058.

(6) Realista, S.; Fitzpatrick, A. J.; Santos, G.; Ferreira, L. P.; Barroso, S.; Pereira, L. C. J.; Bandeira, N. A. G.; Neugebauer, P.; Hruby, J.; Morgan, G. G.; van Slageren, J.; Calhorda, M. J.; Martinho, P. N. A Mn(III) single ion magnet with tridentate Schiff-base ligands. *Dalton Trans.* **2016**, *45*, 12301−12307.

(7) Dolai, M.; Mondal, A.; Liu, J.-L.; Ali, M. Three Novel Mononuclear Mn(III)-Based Magnetic Materials With Square Pyramidal Versus Octahedral Geometries. *New J. Chem.* **2017**, *41*, 10890−10898.

(8) Ishikawa, R.; Miyamoto, R.; Nojiri, H.; Breedlove, B. K.; Yamashita, M. Slow Relaxation of the Magnetization of an Mn^{III} Single Ion. *Inorg. Chem.* **2013**, *52*, 8300−8302.

(9) Vallejo, J.; Pascual-Alvarez, A.; Cano, J.; Castro, I.; Julve, M.; Lloret, F.; Krzystek, J.; De Munno, G.; Armentano, D.; Wernsdorfer, W.; Ruiz-Garcia, R.; Pardo, E. Field-Induced Hysteresis and Quantum Tunneling of the Magnetizationin a Mononuclear Manganese(III) Complex. *Angew. Chem., Int. Ed.* **2013**, *52*, 14075−14079.

(10) Sun, H. L.; Wang, Z. M.; Gao, S. Strategies towards single-chain magnets. *Coord. Chem. Rev.* **2010**, *254*, 1081−1100.

(11) Bar, A. K.; Pichon, C.; Sutter, J. P. Magnetic anisotropy in two- to eight-coordinated transition-metal complexes: recent developments in molecular magnetism. *Coord. Chem. Rev.* **2016**, *308*, 346−380.

(12) Giannopoulos, D. P.; Thuijs, A.; Wernsdorfer, W.; Pilkington, M.; Christou, G.; Stamatatos, T. C. Supramoleculr chains of high nuclearity $\{Mn^{III}{}_{25}\}$ barrel-like single molecule magnets. *Chem. Commun.* **2014**, *50*, 779−781.

(13) Silha, T.; Nemec, I.; Herchel, R.; Travnicek, Z. Structural and magnetic characterizations of the first manganese(III) Schiff base complexes involving hexathiocyanidoplatinate(IV) bridges. *CrystEngComm* **2013**, *15*, 5351−5358.

(14) Weatherburn, D. C.; Mandal, S.; Mukhopadhyay, S.; Bhaduri, S.; Lindoy, L. F. *Manganese, in Comprehensive Coordination Chemistry II: From Biology to Nanotechnology*, 2nd ed.; Constable, E.C., Dilworth, J. R., Eds.; Elsevier, 2005; Vol. 5.

(15) Stetsiuk, O.; Synytsia, V.; Petrusenko, S. R.; Kokozay, V. N.; El-Ghayoury, A.; Cano, J.; Lloret, F.; Julve, M.; Fleury, B.; Avarvari, N. Co-existence of ferro- and antiferromagnetic interactions in a hexanuclear mixed-valence $Co^{III}{}_2Mn^{II}{}_2Mn^{IV}{}_2$ cluster sustained by a multidentate Schiff base ligand. *Dalton Trans.* **2019**, *48*, 11862−11871.

(16) Nesterova, O. V.; Chygorin, E. N.; Kokozay, V. N.; Omelchenko, I. V.; Shishkin, O. V.; Boca, R.; Pombeiro, A. J. L. A self-assembled octanuclear complex bearing the uncommon close-packed $\{Fe_4Mn_4(\mu_4\text{-}O)_4(\mu\text{-}O)_4\}$ molecular core. *Dalton Trans.* **2015**, *44*, 14918−14924.

(17) Kokozay, V. N.; Vassilyeva, O. Y.; Makhankova, V. G. *Direct Synthesis of Metal Complexes*; Kharisov, B., Ed.; Elsevier: Amsterdam, 2018; pp 183−237.

(18) Nesterov, D. S.; Nesterova, O. V.; Kokozay, V. N.; Pombeiro, A. J. L. Polynuclear Heterometallic Complexes from Metal Powders: The "Direct Synthesis" Approach. *Eur. J. Inorg. Chem.* **2014**, *2014*, 4496−4517.

(19) Zhang, L. F.; Ni, Z. H.; Zong, Z. M.; Wei, X. Y.; Ge, C. H.; Kou, H. Z. A novel one-dimensional complex: catena-poly-[[manganese(III)-di-μ-2-[(2-hydroxyethyl)iminomethyl]phenolato-$\kappa^2O^1,N:\kappa O^2;\kappa O^2:\kappa^2O^1$]chloride]. *Acta Crystallogr.* **2005**, *C61*, m542−m544.

(20) Petrusenko, S. R.; Stetsyuk, O. M.; Omelchenko, I. V. Catena-Poly[[manganese(III)-bis{[mu]-2-[(2-hydroxyethyl)iminomethyl]-6-methoxyphenolato- $\kappa^3O^1,N:O^2;\kappa^3O^2:N,O^1$}] iodide]. *Acta Crystallogr.* **2013**, *E69*, m326−m327.

(21) Brown, I. D.; Altermatt, D. Bond-Valence Parameters Obtained from a Systematic Analysis of the Inorganic Crystal Structure Database. *Acta Crystallogr., Sect. B: Struct. Sci.* **1985**, *41*, 244−247.
(22) Thorp, H. H. Bond Valence Sum Analysis of Metal-Ligand Bond Lengths in Metalloenzymes and Model Complexes. *Inorg. Chem.* **1992**, *31*, 1585−1588.
(23) Coxall, R. A.; Harris, S. G.; Henderson, D. K.; Parsons, S.; Tasker, P. A.; Winpenny, R. E. P. Inter-ligand reactions: in situ formation of new polydentate ligands. *J. Chem. Soc., Dalton Trans.* **2000**, 2349−2356.
(24) Collin, R. J.; Smith, B. C. Ionic Radii for Group 1 Halide Crystals and Ion-Pairs. *Dalton Trans.* **2005**, *4*, 702−705.
(25) Campbell, K. A.; Force, D. A.; Nixon, P. J.; Dole, F.; Diner, B. A.; Britt, R. D. Dual-Mode EPR Detects the Initial Intermediate in Photoassembly of the Photosystem II Mn Cluster: The Influence of Amino Acid Residue 170 of the D1 Polypeptide on Mn Coordination. *J. Am. Chem. Soc.* **2000**, *122*, 3754−3761.
(26) Campbell, K. A.; Lashley, M. R.; Wyatt, J. K.; Nantz, M. H.; Britt, R. D. Dual-Mode EPR Study of Mn(III) Salen and the Mn(III) Salen-Catalyzed Epoxidation of *cis*-β-Methylstyrene. *J. Am. Chem. Soc.* **2001**, *123*, 5710−5719.
(27) Gupta, R.; Taguchi, T.; Borovik, A. S.; Hendrich, M. P. Characterization of Monomeric MnII/III/IV-Hydroxo Complexes from X- and Q-Band Dual Mode Electron Paramagnetic Resonance (EPR) Spectroscopy. *Inorg. Chem.* **2013**, *52*, 12568−12575.
(28) Westphal, A.; Klinkebiel, A.; Berends, H. M.; Broda, H.; Kurz, P.; Tuczek, F. Electronic Structure and Spectroscopic Properties of Mononuclear Manganese(III) Schiff Base Complexes: A Systematic Study on [Mn(acen)X] Complexes by EPR, UV/vis, and MCD Spectroscopy (X = Hal, NCS). *Inorg. Chem.* **2013**, *52*, 2372−2387.
(29) Oswald, V. F.; Weitz, A. C.; Biswas, S.; Ziller, J. W.; Hendrich, M. P.; Borovik, A. S. Manganese - Hydroxido Complexes Supported by a Urea/Phosphinic Amide Tripodal Ligand. *Inorg. Chem.* **2018**, *57*, 13341−13350.
(30) Aromi, G.; Telser, J.; Ozarowski, A.; Brunel, L. C.; Stoeckli-Evans, H. M.; Krzystek, J. Synthesis, Crystal Structure, and High-Precision High-Frequency and - Field Electron Paramagnetic Resonance Investigation of a Manganese(III) Complex: $[Mn(dbm)_2(py)_2](ClO_4)$. *Inorg. Chem.* **2005**, *44*, 187−196.
(31) Duboc, C. Determination and Prediction of The Magnetic Anisotropy of Mn Ions. *Chem. Soc. Rev.* **2016**, *45*, 5834−5847.
(32) Arauzo, A.; Bartolomé, E.; Benniston, A. C.; Melnic, S.; Shova, S.; Luzón, J.; Alonso, P. J.; Barra, A. L.; Bartolomé, J. Slow Magnetic Relaxation In A Dimeric Mn_2Ca_2 Complex Enabled By The Large Mn(III) Rhombicity. *Dalton Trans.* **2017**, *46*, 720−732.
(33) Konstantatos, A.; Bewley, R.; Barra, A. L.; Bendix, J.; Piligkos, S.; Weihe, H. In-Depth Magnetic Characterization of a [2 × 2] Mn(III) Square Grid Using SQUID Magnetometry, Inelastic Neutron Scattering, and High Field Electron Paramagnetic Resonance Spectroscopy. *Inorg. Chem.* **2016**, *55*, 10377−10382.
(34) Ozarowski, A. The Zero-Field-Splitting Parameter D in Binuclear Copper(II) Carboxylates Is Negative. *Inorg. Chem.* **2008**, *47*, 9760−9762.
(35) Ozarowski, A.; Calzado, C. J.; Sharma, R. P.; Kumar, S.; Jezierska, J.; Angeli, C.; Spizzo, F.; Ferretti, V. Metal-Metal Interactions in Trinuclear Copper(II) Complexes $[Cu_3(RCOO)_4(H_2TEA)_2]$ and Binuclear $[Cu_2(RCOO)_2(H_2TEA)_2]$. Syntheses and Combined Structural, Magnetic, High-Field Electron Paramagnetic Resonance, and Theoretical Studies. *Inorg. Chem.* **2015**, *54*, 11916−11934.
(36) Ozarowski, A.; Szymanska, I. B.; Muziol, T.; Jezierska, J. High-Field EPR and Magnetic Susceptibility Studies on Binuclear and Tetranuclear Copper Trifluoroacetate Complexes. X-ray Structure Determination of Three Tetranuclear Quinoline Adducts of Copper-(II) Trifluoroacetate. *J. Am. Chem. Soc.* **2009**, *131*, 10279−10292.
(37) Boca, R. Zero-field splitting in metal complexes. *Coord. Chem. Rev.* **2004**, *248*, 757−815.
(38) Boca, R. Magnetic Parameters and Magnetic Functions in Mononuclear Complexes Beyond the Spin-Hamiltonian Formalism. *Struct. Bonding (Berlin)* **2006**, *117*, 1−264.
(39) Tadyszak, K.; Rudowicz, C.; Ohta, H.; Sakurai, T. Electron magnetic resonance data on high-spin Mn(III; S= 2) ions in porphyrinic and salen complexes modeled by microscopic spin Hamiltonian approach. *J. Inorg. Biochem.* **2017**, *175*, 36−46.
(40) Mossin, S.; Weihe, H.; Barra, A. L. Is the Axial Zero-Field Splitting Parameter of Tetragonally Elongated High-Spin Manganese-(III) Complexes Always Negative? *J. Am. Chem. Soc.* **2002**, *124*, 8764−8765.
(41) Shova, S.; Vlad, A.; Cazacu, M.; Krzystek, J.; Bucinsky, L.; Breza, M.; Darvasiova, D.; Rapta, P.; Cano, J.; Telser, J.; Arion, V. B. A five-Coordinate Manganese(III) Complex Of A Salen Type Ligand With A Positive Axial Anisotropy Parameter D. *Dalton Trans.* **2017**, *46*, 11817−11829.
(42) Duboc, C.; Ganyushin, D.; Sivalingam, K.; Collomb, M.-N.; Neese, F. Systematic Theoretical Study of the Zero-Field Splitting in Coordination Complexes of Mn(III). Density Functional Theory versus Multireference Wave Function Approaches. *J. Phys. Chem. A* **2010**, *114*, 10750−10758.
(43) Pascual-Alvarez, A.; Vallejo, J.; Pardo, E.; Julve, M.; Lloret, F.; Krzystek, J.; Armentano, D.; Wernsdorfer, W.; Cano, J. Field-Induced Slow Magnetic Relaxation in a Mononuclear Manganese(III)-Porphyrin Complex. *Chem. - Eur. J.* **2015**, *21*, 17299−17307.
(44) Schäfer, A.; Horn, H.; Ahlrichs, R. Fully Optimized Contracted Gaussian Basis Sets for Atoms Li to Kr. *J. Chem. Phys.* **1992**, *97*, 2571−2577.
(45) The Ahlrichs auxiliary basis sets were obtained from the TurboMole basis set library under ftp.chemie.uni-karlsruhe.de/pub/jbasen.
(46) Eichkorn, K.; Weigend, F.; Treutler, O.; Ahlrichs, R. Auxiliary Basis Sets for Main Row Atoms and Transition Metals and Their Use to Approximate Coulomb Potentials. *Theor. Chem. Acc.* **1997**, *97*, 119−124.
(47) Neese, F. *ORCA - An Ab Initio, Density Functional and Semiempirical Program Package*, Version 4.0.1; Surf Sara: Amsterdam, 2017. Neese, F. The ORCA Program System. *Wiley Interdiscip. Rev.: Comput. Mol. Sci.* **2012**, *2*, 73−78.
(48) Harvey, J. D.; Ziegler, C. J.; Telser, J.; Ozarowski, A.; Krzystek, J. High-Frequency and - Field EPR Investigation of a Manganese(III) N-Confused Porphyrin Complex, $[Mn(NCTPP)(py)_2]$. *Inorg. Chem.* **2005**, *44*, 4451−4453.
(49) Pascual-Álvarez, A.; Vallejo, J.; Pardo, E.; Julve, M.; Lloret, F.; Krzystek, J.; Armentano, D.; Wernsdorfer, W.; Cano, J. Field-induced slow magnetic relaxation in a mononuclear manganese(III) porphyrin. *Chem. - Eur. J.* **2015**, *21*, 17299−17307.
(50) Noodleman, L. Valence Bond Description of Antiferromagnetic Coupling in Transition Metal Dimers. *J. Chem. Phys.* **1981**, *74*, 5737−5743.
(51) Noodleman, L.; Davidson, E. R. Ligand Spin Polarization and Antiferromagnetic Coupling in Transition Metal Dimers. *Chem. Phys.* **1986**, *109*, 131−143.
(52) Malrieu, J. P.; Caballol, R.; Calzado, C. J.; de Graaf, C.; Guihéry, N. Magnetic Interactions in Molecules and Highly Correlated Materials: Physical Content, Analytical Derivation, and Rigorous Extraction of Magnetic Hamiltonians. *Chem. Rev.* **2014**, *114*, 429−492.
(53) Rodríguez-Fortea, A.; Alemany, P.; Alvarez, S.; Ruiz, E. Exchange Coupling in Halo-Bridged Dinuclear Cu(II) Compounds: A Density Functional Study. *Inorg. Chem.* **2002**, *41*, 3769−3778.
(54) Aromi, G.; Gamez, P.; Roubeau, O.; Berzal, P. C.; Kooijman, H.; Spek, A. L.; Driessen, W. L.; Reedijk, J. A Solvent-Controlled Switch of Manganese Complex Assemblies with a β-Diketonate-Based Ligand. *Inorg. Chem.* **2002**, *41*, 3673−3683.
(55) Shova, S.; Vlad, A.; Cazacu, M.; Krzystek, J.; Ozarowski, A.; Malcek, M.; Bucinsky, L.; Rapta, P.; Cano, J.; Telser, J.; Arion, V. B. Dinuclear manganese(III) complexes with bioinspired coordination and variable linkers showing weak exchange effects: a synthetic,

https://dx.doi.org/10.1021/acs.cgd.9b01150
Cryst. Growth Des. 2020, 20, 1491−1502

structural, spectroscopic and computation study. *Dalton Trans.* **2019**, *48*, 5909−5922.
(56) Hassan, A.; Pardi, L.; Krzystek, J.; Sienkiewicz, A.; Goy, P.; Rohrer, M.; Brunel, L.-C. Ultrawide Band Multifrequency High-Field EMR Technique: A Methodology for Increasing Spectroscopic Information. *J. Magn. Reson.* **2000**, *142*, 300−312.

https://dx.doi.org/10.1021/acs.cgd.9b01150
Cryst. Growth Des. 2020, 20, 1491−1502